The Transition to Three-Dimensionality in the Flow Produced by an Oscillating Circular Cylinder

J. R. Elston[1], J. Sheridan[1] and H. M. Blackburn[2]

[1]Department of Mechanical Engineering
Monash University, Victoria, 3800 AUSTRALIA

[2]CSIRO Building, Construction & Engineering
PO Box 56, Highett, Victoria, 3190 AUSTRALIA

Abstract

The stability of the flow generated by a cylinder oscillating in quiescent fluid is investigated using direct numerical simulation and Floquet analysis. This study determines transitions between flow regimes as functions of the dimensionless oscillation amplitude (Keulegan-Carpenter number, KC) and frequency (Stokes number, β). At low values of KC and β the flow is two-dimensional and has a reflection symmetry about the axis of oscillation. Increasing KC or β causes either of two distinct transitions to three-dimensional flow. The two transitions are either a breakage in the reflection symmetry accompanied by a three-dimensional transition or a transition to three-dimensional flow where the spanwise average maintains the original symmetry. The interaction of these two transitions results in a large number of complex vortex shedding patterns which were visualised in the experimental studies of Tatsuno & Bearman [5]. Accurate locations of the transitions and the variation of the three-dimensional critical wavelength as a function of KC and β are presented.

Introduction

Oscillatory motion of a circular cylinder normal to its axis in quiescent fluid generates a streaming motion of the fluid. In the case of an infinitely long cylinder, two dimensionless control parameters determine the state of the flow. These are the Keulegan–Carpenter number $KC = 2\pi a/D$ and the Stokes number $\beta = fD^2/\nu$, where a is the amplitude of motion, D is the cylinder diameter and f is the frequency of oscillation. A Reynolds number can be defined as $Re = \beta KC$.

Several well-defined and fascinating two- and three-dimensional structures have been shown to occur in this flow. Honji [3] used flow visualisation to show that the appearance of streaks that alternated along the length of the cylinder axis was evidence of a three-dimensional spanwise instability. Tatsuno & Bearman [5] further extended this work and produced a control-space map, classifying the flows into eight separate flow regimes each with a characteristic two- and three-dimensional flow structure. Numerical simulations of these phenomena to date have only examined the two-dimensional transition that occurs for low KC and β values. Iliadis & Anagnostopoulos [4] used a finite element method to locate the boundary between symmetric and asymmetric two-dimensional flow.

The characteristics of the flow regimes defined by [5] can be described in terms of their symmetry properties. At the boundaries between these regimes a transition in the symmetry properties occurs. At very low values of KC and β the flow resulting from a cylinder oscillating in the vertical (y) axis has the following symmetry properties:

$$u(x,y,z,t) = -u(-x,y,z,t) \tag{1a}$$
$$v(x,y,z,t) = v(-x,y,z,t) \tag{1b}$$
$$u(x,y,z,t) = u(x,-y,z,t+T/2) \tag{2a}$$
$$v(x,y,z,t) = -v(x,-y,t+T/2) \tag{2b}$$
$$\boldsymbol{u}(x,y,z,t) = \boldsymbol{u}(x,y,z,t+T) \tag{3}$$
$$\boldsymbol{u}(x,y,z,t) = \boldsymbol{u}(x,y,z+Z,t) \tag{4}$$

where $\boldsymbol{u} = (u,v,w)$, T is the period of oscillation and Z is an arbitrary translation along the z-axis. Reflection symmetry about the y-axis is represented by (1), while (2) represents a symmetry about the x-axis which is the same as that observed about the wake centreline for von Kármán vortex shedding. Equation (3) results from the periodic nature of the oscillation and (4) represents the spanwise (z-axis) translation symmetry.

The purpose of this study is to apply a combination of direct numerical simulation and Floquet stability analysis [1] to determine the locations of the two- and three-dimensional transitions and accurately quantify the critical wavelengths at which three-dimensional transitions occur.

Computational Methods

The direct numerical simulations (DNS) presented in this paper employed a spectral element spatial discretisation to solve the two-dimensional (2D) incompressible Navier–Stokes equations in an accelerating reference frame attached to the cylinder [2]. The three-dimensional (3D) simulations utilised Fourier expansions along the axis of the cylinder; this provides a domain that is periodic in the spanwise direction.

The stability of the two-dimensional time-periodic solutions found using DNS is obtained via Floquet stability analysis. This method determines the stability of a two-dimensional time-periodic base flow to infinitesimal disturbances in either two or three dimensions. In the cases described here this is achieved using the linearised Navier–Stokes equations as a subroutine to an Arnoldi-method eigensystem solver to extract the leading eigenpairs [6]. The linearised Navier–Stokes equations are:

$$\frac{\partial \boldsymbol{u}'}{\partial t} = -\boldsymbol{u}' \cdot \nabla \boldsymbol{U} - \boldsymbol{U} \cdot \nabla \boldsymbol{u}' - \frac{1}{\rho}\nabla p' + \frac{1}{Re}\nabla^2 \boldsymbol{u}' \tag{5}$$
$$\nabla \cdot \boldsymbol{u}' = 0$$

where $\boldsymbol{U}(x,y,t)$ is the 2D flow of period T whose stability is sought [1]. $\boldsymbol{u}'(x,y,z,t)$ and $p'(x,y,z,t)$ are the perturbations to the velocity and pressure. The 2D periodic base flow $\boldsymbol{U}$ is reconstructed using Fourier interpolation
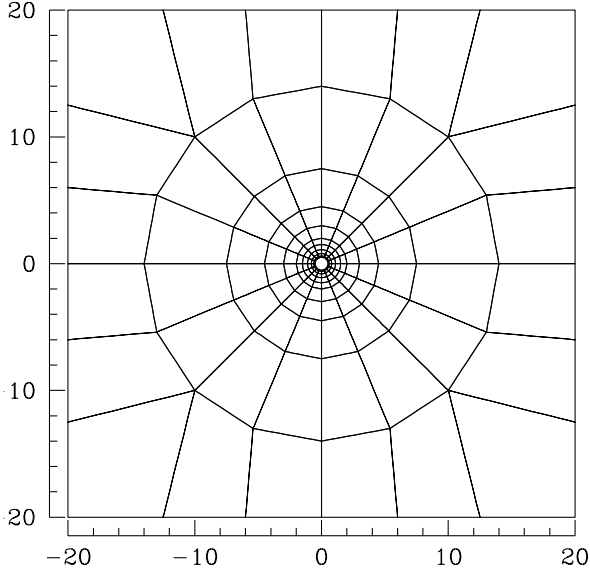
Figure 1: Spectral element mesh used for computations

	Mesh Size	40×40	60×60	80×80
(a)	$\widehat{C}_f$	3.78341	3.78210	3.78045
(b)	p	6	8	10
	$\widehat{C}_f$	3.78420	3.78341	3.78392

Table 1: Convergence results for peak coefficients of force at (a) different mesh sizes at $p = 8$, (b) different interpolant orders with a 40×40 mesh. p is the order of the tensor-product interpolant function employed within each spectral element.

from a sequence of 32 field dumps, obtained via DNS, equally spaced in time over one period.

The breakage of the 2D reflection symmetry of the flow was determined by taking an integral of the product of the velocity component normal to the axis of oscillation multiplied by the distance from the axis over the computational domain Ω:

$$S = \int |x| u(x, y, t) \, \mathrm{d}\Omega \qquad (6)$$

A significant deviation from zero was taken to indicate a transition. The 2D computations employed the DNS code.

In all the results described here, solutions were obtained in a square domain of size $40D \times 40D$ with an interpolant order of 8, using the 164-element mesh shown in figure 1. The outer mesh boundary conditions are set to the prescribed velocity of the mesh. Convergence tests for the mesh size and order of the interpolants are shown in table 1 for control values of $KC = 2.5$, $\beta = 100.0$.

Two-Dimensional Symmetry-Breaking

Here we examine the breaking of the 2D reflection symmetry about the oscillation axis using 2D DNS. A transition from the streaming flow along the cylinder axis occurs as the parameters KC and β are increased [3, 5]. The initial state has symmetries about both the x and y-axes, is periodic in time and is two-dimensional as described by (1–4). Figure 2 shows the vorticity contours for this symmetrical state. Two possible transitions were
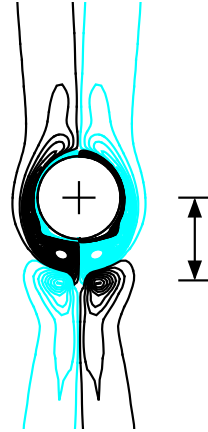

Figure 2: Close up of vorticity contours for the flow produced by a cylinder in vertical oscillation. Also shown is the peak-to-peak amplitude of oscillation. At $KC = 3.5$ and $\beta = 100.0$ the vorticity contours exhibit reflection symmetry about the oscillation axis.

found to occur as the controlling parameters were increased. The first was a transition from the state of figure 2 to that shown in figure 3. In this case the reflection symmetry, (1), has been broken and the induced flow no longer streams along the oscillation axis but makes an angle to the oscillation direction. However the flow retains the remaining symmetry properties (2–4).
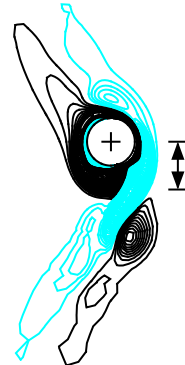

Figure 3: Close up of vorticity contours for the flow produced by a cylinder in vertical oscillation. Also shown is the peak-to-peak amplitude of oscillation. At $KC = 6.0$ and $\beta = 22.5$ the reflection symmetry seen in figure 2 has been broken.

The second transition was from the initial state of figure 2 to that shown in figure 4. In this case, both the reflection symmetry and the periodic symmetry about the x-axis have been broken, as described by (1–3). The direction of flow convection switches chaotically from either side of the vertical axis so that vorticity contours such as those seen in figure 4 occur. However the initial stages of the simulations resembled the flow in figure 3 as found by Tatsuno & Bearman [5] before becoming chaotic.

A large number of simulations utilising the measure of symmetry from (6) were used to determine the boundary in the (KC, β) control space between the symmetrical and asymmetrical flows. The results of figure 5 show the location of this transition. The transition to the state shown in figure 3 occurs in the upper branch for low β and high KC values while the transition to the aperiodic state of figure 4 occurs for the branch with low
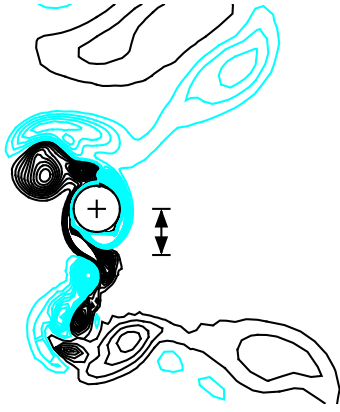
Figure 4: Close up of vorticity contours for the flow produced by a cylinder in vertical oscillation. Also shown is the peak-to-peak amplitude of oscillation. At $KC = 4.0$ and $\beta = 100.0$ the two-dimensional symmetry properties exhibited in figure 2 have been lost.

KC values. These are in excellent agreement with existing experimental results [5] but differ slightly from the numerical results [4]. The difference could possibly be attributed to the smaller domain ($20D \times 20 - 40D$) or to the different technique (finite element method) employed in obtaining those results.
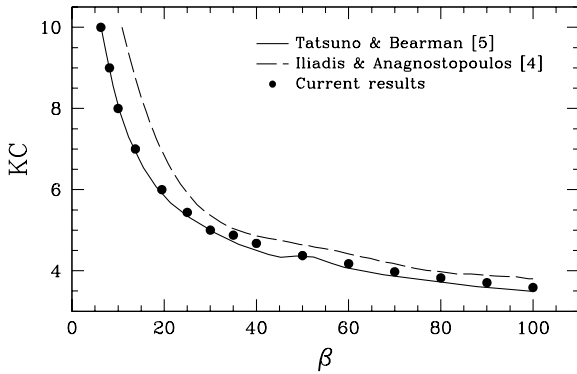
Figure 5: Results for the first 2D transition in the symmetry characteristics of the flow as the controlling parameters are increased. Also shown is the regime boundary for 2D transition of Tatsuno & Bearman [5] and of Iliadis & Anagnostopoulos [4].

Three-Dimensional Symmetry-Breaking

In this section we examine the onset of three-dimensionality which is the breakage of the spanwise symmetry property (4). Determination of the transition location was achieved using Floquet analysis. Figure 6 shows an example where the critical wavenumber is determined as a function of β for $KC = \pi$. In this instance the transition to three-dimensionality occurred at $\beta = 57.5$, $KC = \pi$ for a critical wavenumber $k = 2\pi D/\lambda$ of 4.5. Figure 7 shows the vorticity isosurfaces of the dominant mode at $KC = \pi$. This compares favorably with the vorticity isosurfaces from three-dimensional DNS run using the matching axial periodic length of $1.40D$, which is shown in figure 8. The differences result mainly from the presence of nonlinear advection terms in the full Navier–Stokes equations, as opposed to their linearised equivalents in (5). For transition at low values of β, the base flow had broken the reflection symmetry property before
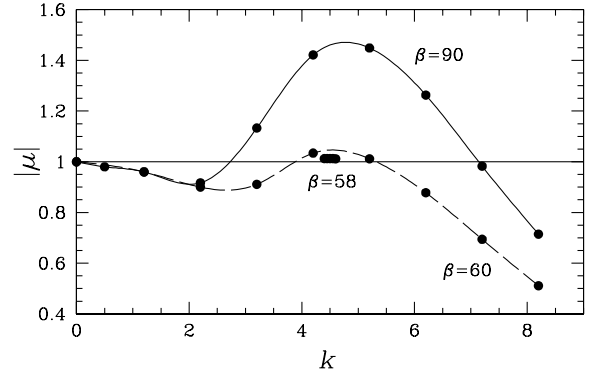

Figure 6: Floquet multiplier μ dependence on spanwise wavenumber k at the given β values for $KC = \pi$. Values of μ greater than 1 indicate the growth of a 3D instability.

a 3D mode became unstable. Figures 9 and 10 show a critical Floquet mode for this region, at $KC = 2\pi$ and $\beta = 18.1$ with the corresponding 3D DNS solution.
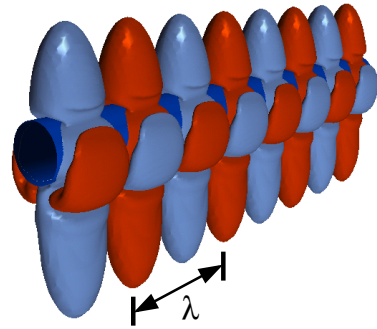

Figure 7: Vorticity isosurfaces of the critical Floquet mode at $KC = \pi$, for the component of vorticity aligned with cylinder translation. Four spanwise-periodic repetitions of wavelength λ are shown.
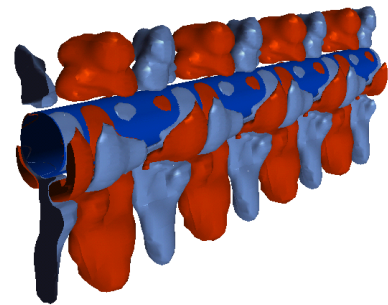

Figure 8: Vorticity isosurfaces generated by three-dimensional DNS at $KC = \pi$. Four periodic repetitions are shown.

The location of the transition to three-dimensionality is shown in figure 11. The results closely match the results of Tatsuno & Bearman [5]. The region in the mid-section of the curve is devoid of points because the 2D base flow was aperiodic in this region and this breaks an essential criterion for the use of Floquet analysis. The critical wavenumbers k at the onset of three-dimensionality, shown in figure 12, quite clearly have two distinct regions which reflect the different 2D base flows at the point of transition.
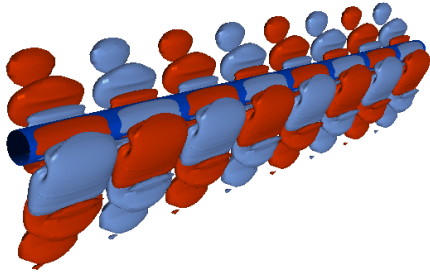
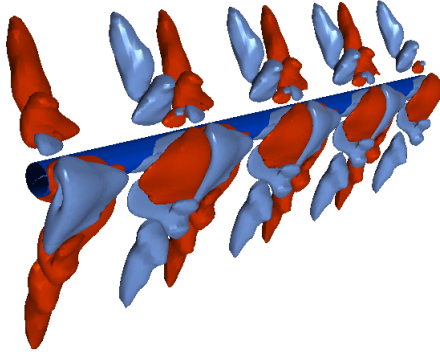Figure 9: Vorticity isosurfaces of the critical Floquet mode at $KC = 2\pi$. Four periodic repetitions are shown.

Figure 10: Vorticity isosurfaces generated by the nonlinear Navier–Stokes solver at $KC = 2\pi$. Four periodic repetitions are shown.
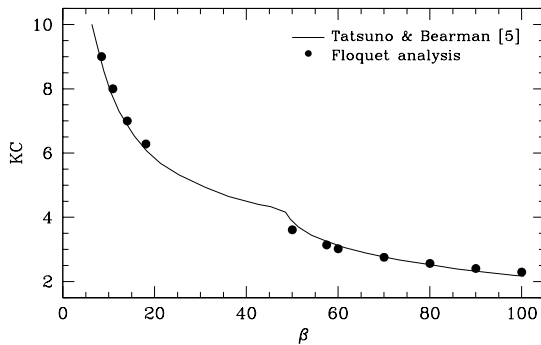

Figure 11: Three-dimensional transition curve denoting the onset of instability. Floquet analysis results and the experimental regime boundary for 3D transition from Tatsuno & Bearman [5] are shown.

Combined Results

Curves representing two- and three-dimensional transition from figures 5 and 11 are overlaid in figure 13 along with the results of Tatsuno & Bearman [5]. Our numerical results clearly match quite closely their experimental results. It is interesting to note that a necessary precondition for 3D instability in the low β, high KC area was a breakage in the reflection symmetry property of the 2D base flow as shown in figure 3.

Conclusions

It has been shown that the transitions in the two-dimensional state and the onset of three-dimensional instabilities of a sinusoidally oscillating circular cylinder can be accurately determined using a combination of 2D DNS and Floquet analysis. The results obtained closely match experimental [5] and numerical [4] results found by other researchers.
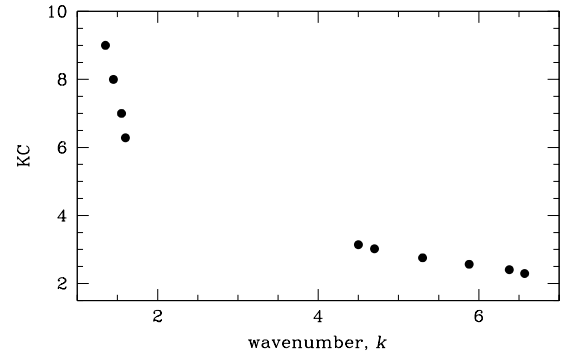

Figure 12: Variation of the critical wavenumber with KC at transition. The two different transitions that occur are clearly shown as two different sets of wavenumbers.
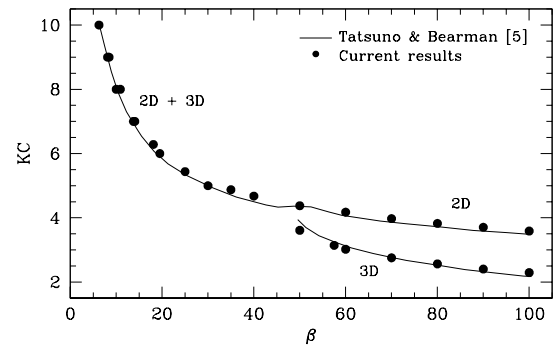

Figure 13: Transition results for both two and three-dimensional cases. Also shown are the corresponding regime boundaries of Tatsuno & Bearman [5].

References

[1] Barkley, D. and Henderson, R. D., Three–dimensional Floquet Stability Analysis of the Wake of a Circular Cylinder, *J. Fluid Mech.*, **322**, 1996, 215–241.

[2] Blackburn, H. M. and Henderson, R. D., A Study of Two-Dimensional Flow Past an Oscillating Cylinder, *J. Fluid Mech.*, **385**, 1999, 255–286.

[3] Honji, H., Streaked flow around an Oscillating Cylinder, *J. Fluid Mech.*, **107**, 1981, 509–520.

[4] Iliadis, G. and Anagnostopoulos, P., Viscous Oscillatory Flow Around a Circular Cylinder at Low Keulegan–Carpenter Numbers and Frequency Parameters, *Intnl J. Num. Meth. Fluids*, **26**, 1998, 403–442.

[5] Tatsuno, M. and Bearman, P. W., A Visual Study of the Flow around an Oscillating Circular Cylinder at Low Keulegan–Carpenter Numbers and Low Stokes Numbers, *J. Fluid Mech.*, **211**, 1990, 157–182.

[6] Tuckerman, L. S. and Barkley, D., Bifurcation Analysis for Timesteppers, in *Numerical Methods for Bifurcation Problems and Large-Scale Dynamical Systems*, editors E. Doedel and L. S. Tuckerman, Springer, New York, 2000, 543–566.